Exploring the exact factorization adapted nonadiabatic dynamics on various potential landscapes

Daeho Han

Department of Chemistry,
University at Buffalo, SUNY

July 8, 2024

Light-induced phenomena & nonadiabatic dynamics

- Nonadiabatic dynamics calculations prevail in simulating various light-induced phenomena.

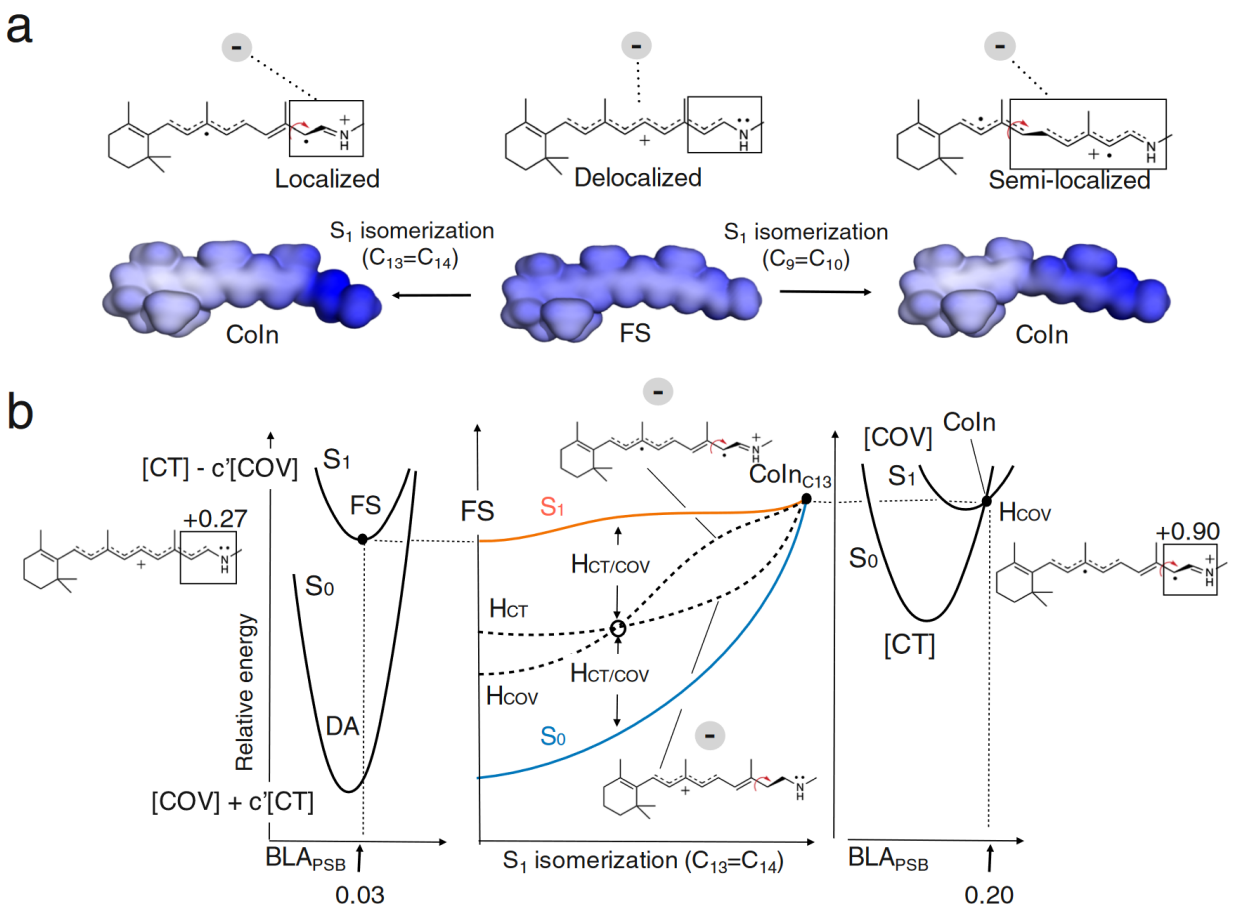

Photophysics of biomolecules

Palombo, R.; Barneschi, L.; Pedraza-González, L.; Padula, D.; Schapiro, I.; Olivucci, M. Nat. Commun. ***2022***, 13 (1), 6652.

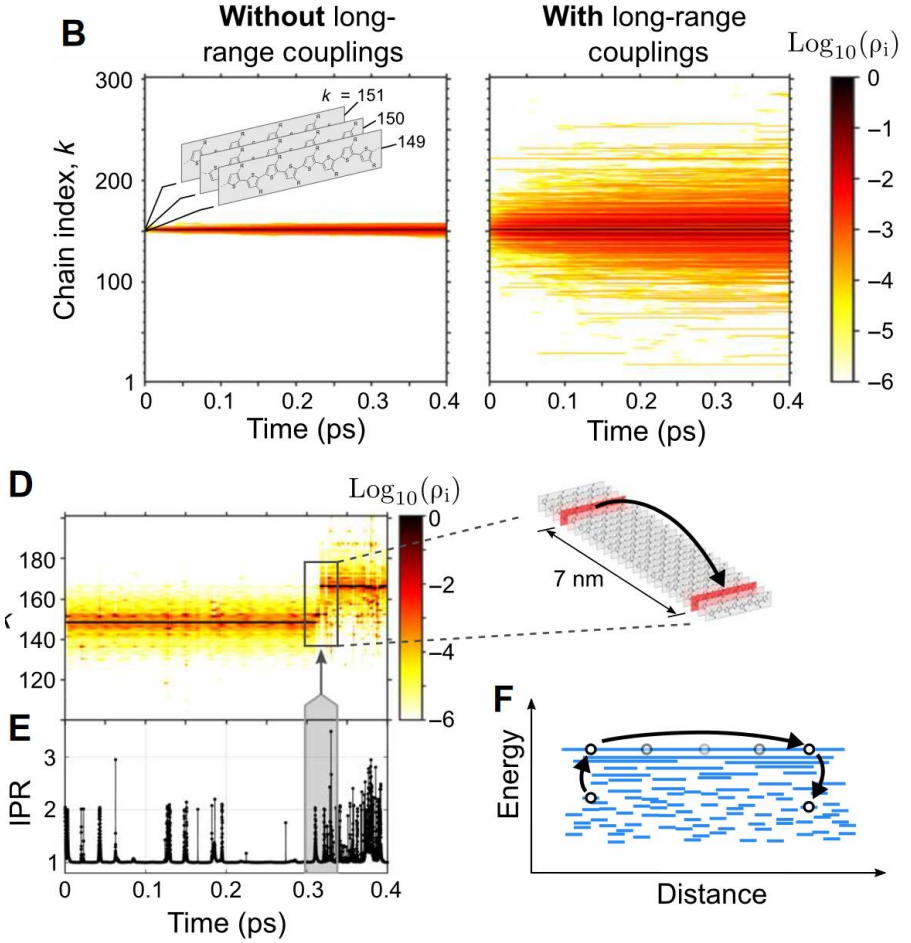

Exciton transfer in organic semiconductors

Sneyd, A. J. ; Fukui, T.; Paleček, D.; Prodhan, S.; Wagner, I.; Zhang, Y.; Sung, J.; Collins, S. M.; Slater, T. J. A.; Andaji-Garmaroudi, Z.; MacFarlane, L. R.; Garcia-Hernandez, J. D.; Wang, L.; Whittell, G. R.; Hodgkiss, J. M.; Chen, K.; Beljonne, D.; Manners, I.; Friend, R. H.; Rao, A. Sci. Adv. ***2021***, 7 (32), eabh4232.

Decoherence-corrected nonadiabatic dynamics

- Various decoherence-corrected nonadiabatic dynamics methods have been developed.

Simplified Decay of Mixing (SDM)

Granucci, G.; Persico, M. JCP. ***2007***, 126 (13), 134114.

$$\tau_{ia} = -\frac{\hbar}{|E_i - E_a|}\left(1 + \frac{C}{E_{kin}}\right)C_i \qquad C_{i\neq a} := C_{i\neq a}\exp\left(-\frac{\Delta t}{t_{ia}}\right)$$

A-FSSH

Jain, A.; Alguire, E.; Subotnik, J. E. JCTC. ***2016***, 12 (11), 5256–5268.

$$\tau_{ij}^{-1} = \frac{\delta\boldsymbol{F}_{ii}\cdot\left(\delta\boldsymbol{R}_{ii} - \delta\boldsymbol{R}_{jj}\right)}{2\hbar} - \frac{2\left|\boldsymbol{d}_{ji}\cdot\left(E_j - E_i\right)\left(\delta\boldsymbol{R}_{ii} - \delta\boldsymbol{R}_{jj}\right)\cdot\boldsymbol{v}\right|}{\hbar\boldsymbol{v}\cdot\boldsymbol{v}}$$

Instantaneous Decoherence Approximation (IDA)

Nelson, T.; Fernandez-Alberti, S.; Roitberg, A. E.; Tretiak, S. JCP. ***2013***, 138 (22), 224111.

Mean-field dynamics with stochastic decoherence (MFSD)

Bedard-Hearn, M. J.; Larsen, R. E.; Schwartz, B. J. JCP. ***2005***, 123 (23), 234106.

$$\tau_i^{-2} = \sum_{\nu}\frac{\left(\boldsymbol{F}_{\nu}(0) - \boldsymbol{F}_{i,\nu}\right)^2}{4a_{\nu}\hbar^2}$$

Decoherence-Induced Surface Hopping (DISH)

Jaeger, H. M.; Fischer, S.; Prezhdo, O. V. JCP. ***2012***, 137 (22), 22A545.

$$\tau_i^{-1} = \sum_{j\neq i}\left|C_j\right|^2 r_{ij}$$

⋮

Nonadiabatic dynamics based on exact factorization

- In the decoherence-corrected methods based on exact factorization (XF), the decoherence correction naturally emerges through the electron-nuclear correlation terms.

XF ansatz $\Psi(\boldsymbol{r},\boldsymbol{R},t) = \chi(\boldsymbol{R},t)\Phi_{\boldsymbol{R}}(\boldsymbol{r},t)$

Partial Normalization Condition

$$\forall \boldsymbol{R} \int |\Phi_{\boldsymbol{R}}(\boldsymbol{r},t)|^2 \, d\boldsymbol{r} = 1$$

Nuclear EOM

$$i\hbar\partial_t \chi(\boldsymbol{R},t) = \left(\sum_\nu \frac{[-i\hbar\nabla_\nu + A_\nu(\boldsymbol{R},t)]^2}{2M_\nu} + \epsilon(\boldsymbol{R},t) \right) \chi(\boldsymbol{R},t)$$

$\epsilon(\boldsymbol{R},t) = \langle \Phi_{\boldsymbol{R}}(t) | H_{BO} + U_{en}^{coup} - i\hbar\partial_t | \Phi_{\boldsymbol{R}}(t) \rangle_{\boldsymbol{r}}$ TDPES $A_\nu(\boldsymbol{R},t) = \langle \Phi_{\boldsymbol{R}}(t) | -i\hbar\nabla_\nu \Phi_{\boldsymbol{R}}(t) \rangle_{\boldsymbol{r}}$ TD vector potential

Electronic EOM

$$i\hbar\partial_t \Phi_{\boldsymbol{R}}(\boldsymbol{r},t) = \left(H_{BO}(r,\boldsymbol{R}) + U_{en}^{coup}[\Phi_{\boldsymbol{R}},\chi] - \epsilon(\boldsymbol{R},t) \right) \Phi_{\boldsymbol{R}}(\boldsymbol{R},t)$$

Electron-nuclear correlation operator

$$U_{en}^{coup}[\Phi_{\boldsymbol{R}},\chi] = \sum_\nu \frac{1}{M_\nu} \left[\frac{[-i\hbar\nabla_\nu - A_\nu(\boldsymbol{R},t)]^2}{2} + \left(\frac{-i\hbar\nabla_\nu \chi}{\chi} + A_\nu(\boldsymbol{R},t) \right) \cdot (-i\hbar\nabla_\nu - A_\nu(\boldsymbol{R},t)) \right]$$

$$U_{en}^{coup} \approx \sum_\nu \frac{1}{M_\nu} \left(\frac{-i\hbar\nabla_\nu \chi}{\chi} + A_\nu(\boldsymbol{R},t) \right) \cdot \left(-i\hbar\nabla_\nu - A_\nu(\boldsymbol{R},t) \right)$$

Min, S. K.; Agostini, F.; Gross, E. K. U. PRL. ***2015***, 115 (7), 073001.

Agostini, F.; Min, S. K.; Abedi, A.; Gross, E. K. U. JCTC. ***2016***, 12 (5), 2127–2143.

Nonadiabatic dynamics based on exact factorization

- XF-based mixed quantum-classical (XF-MQC) equations

$$i\hbar\dot{\Phi}_{\boldsymbol{R}}(\boldsymbol{r},t)=\left(H_{BO}(r,\boldsymbol{R})-\sum_{\nu}\frac{\mathcal{P}_{\nu}}{M_{\nu}}\cdot\left(A_{\nu}(\boldsymbol{R},t)+i\hbar\nabla_{\nu}\right)\right)\Phi_{\boldsymbol{R}}(\boldsymbol{r},t)$$

$$\boldsymbol{F}_{\nu}=-\langle\Phi_{\boldsymbol{R}}(t)|\nabla_{\nu}H_{BO}|\Phi_{\boldsymbol{R}}(t)\rangle_{\boldsymbol{r}}+\sum_{\mu}\frac{2i\mathcal{P}_{\mu}}{\hbar M_{\mu}}\cdot\left(A_{\mu}(\boldsymbol{R},t)A_{\nu}(\boldsymbol{R},t)-\hbar^{2}\left\langle\nabla_{\mu}\Phi_{\boldsymbol{R}}(t)\middle|\nabla_{\nu}\Phi_{\boldsymbol{R}}(t)\right\rangle_{\boldsymbol{r}}\right)$$

Quantum momentum $\quad\mathcal{P}_{\nu}=-i\hbar\dfrac{\nabla_{\nu}|\chi(\boldsymbol{R},t)|}{|\chi(\boldsymbol{R},t)|}$

Beyond the conventional Ehrenfest terms, the resulting coupled TDSEs explicitly contain the electron-nuclear correlation terms proportional to quantum momenta

Min, S. K.; Agostini, F.; Gross, E. K. U. PRL ***2015***, 115 (7), 073001.

Agostini, F.; Min, S. K.; Abedi, A.; Gross, E. K. U. JCTC ***2016***, 12 (5), 2127–2143.

Nonadiabatic dynamics based on exact factorization

- The XF-MQC equations with the adiabatic basis expansion

$$\dot{C}_i = -\frac{i}{\hbar} E_i C_i - \sum_j C_j \sum_\nu \frac{P_\nu}{M_\nu} \cdot d_{ij,\nu} + \sum_\nu \frac{i\mathcal{P}_\nu}{\hbar M_\nu} \cdot \left(\sum_j |C_j|^2 \phi_{j\nu} - \phi_{i\nu} \right) C_i$$

$$F_\nu = -\sum_i \rho_{ii} \nabla_\nu E_i - \sum_{ij} \rho_{ij} (E_j - E_i) d_{ij,\nu} + \sum_{ij} \rho_{ii}\rho_{jj} \left[\sum_\mu \frac{2i\mathcal{P}_\mu}{\hbar M_\mu} \cdot (\phi_{j,\mu} - \phi_{i,\mu}) \right] \phi_{i,\nu}$$

Phase gradient $\phi_{i,\nu}$ $\quad C_i = |C_i| \exp\left(\frac{i}{\hbar}\theta_i\right) \quad \nabla_\nu \theta_i = \phi_{i,\nu}$

Min, S. K.; Agostini, F.; Gross, E. K. U. PRL ***2015***, 115 (7), 073001.

Agostini, F.; Min, S. K.; Abedi, A.; Gross, E. K. U. JCTC ***2016***, 12 (5), 2127–2143.

Independent-trajectory XF methods

- Approximations to the XF quantities with the auxiliary trajectories
  - Aux. trajectories are generated for each adiabatic state to reflect on the overall nuclear distribution without using other trajectory information.
  - Aux. positions are propagated by aux. momentum determined by the energy conservation and scaling.

$$\boldsymbol{R}_i(t+\Delta t) = \boldsymbol{R}_i(t) + \boldsymbol{M}^{-1}\boldsymbol{P}_i(t)\Delta t \qquad \frac{1}{2}\boldsymbol{P}_i^T\boldsymbol{M}^{-1}\boldsymbol{P}_i + E_i = \frac{1}{2}\boldsymbol{P}^T\boldsymbol{M}^{-1}\boldsymbol{P} + E$$

$$\boldsymbol{P}_i = \alpha_i \boldsymbol{P}$$

$$|\chi|^2 = \sum_i |\chi_i|^2 = \sum_i N_i \prod_\nu \exp\left(-\frac{\left(R_\nu - R_{i,\nu}\right)^2}{2\sigma_{i,\nu}^2}\right)$$

$$\mathcal{P}_\nu \approx \frac{i\hbar}{2\sigma_\nu^2}\left(R_\nu - \langle R_\nu \rangle\right) \approx \frac{i\hbar}{2\sigma_\nu^2}\left(R_{a,\nu} - \sum_i \rho_{ii} R_{i,\nu}\right)$$

$$\phi_{i,\nu}(t) \approx \int_{t_i}^{t} -\nabla_\nu E_i\,(t')dt' = P_i(t) - P_i(t_i)$$

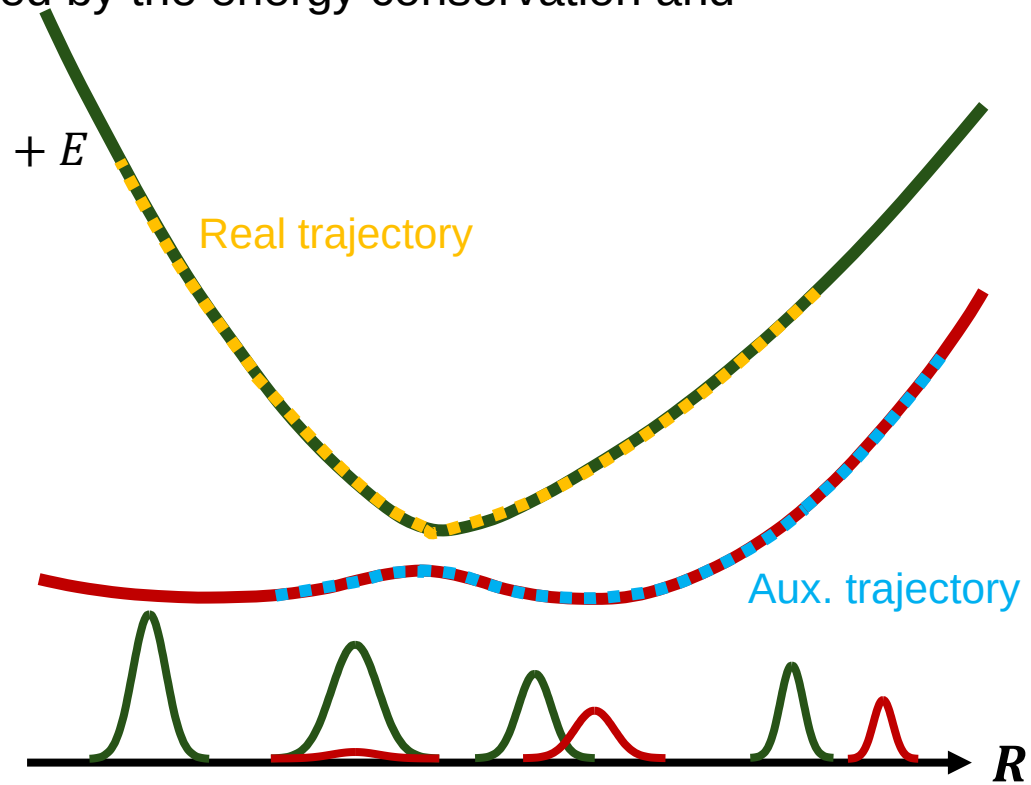

Ha, J.-K.; Lee, I. S.; Min, S. K. JPCL. ***2018***, 9 (5), 1097–1104.

Ha, J.-K.; Min, S. K. JCP. ***2022***, 156 (17), 174109.

Independent-trajectory XF methods

- Branching corrections in aux. propagation

  When the dynamics encounter a classical turning point, the density is projected out or collapsed to remove wrong behaviors of aux. trajectories.

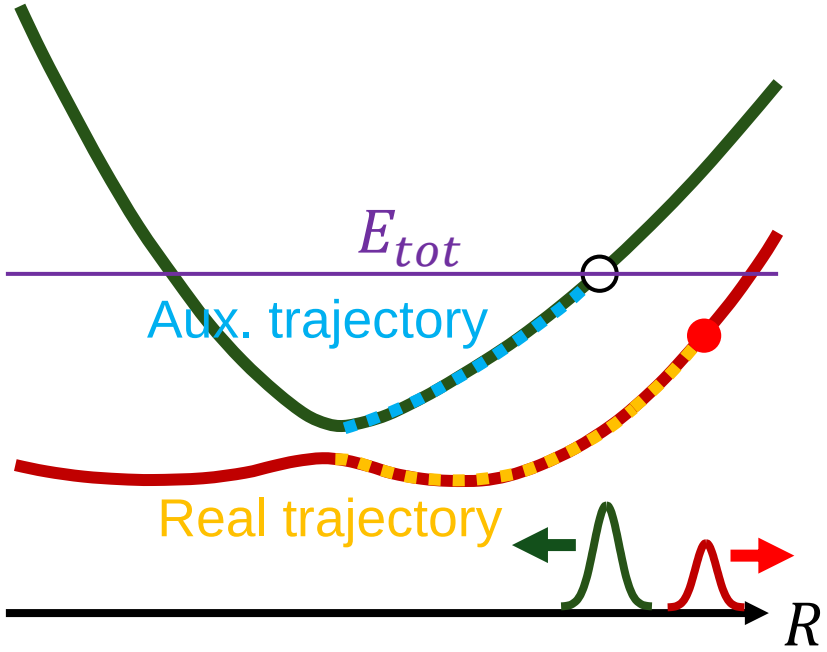

Case I. An auxiliary trajectory encounters the turning point.

Project out the auxiliary density

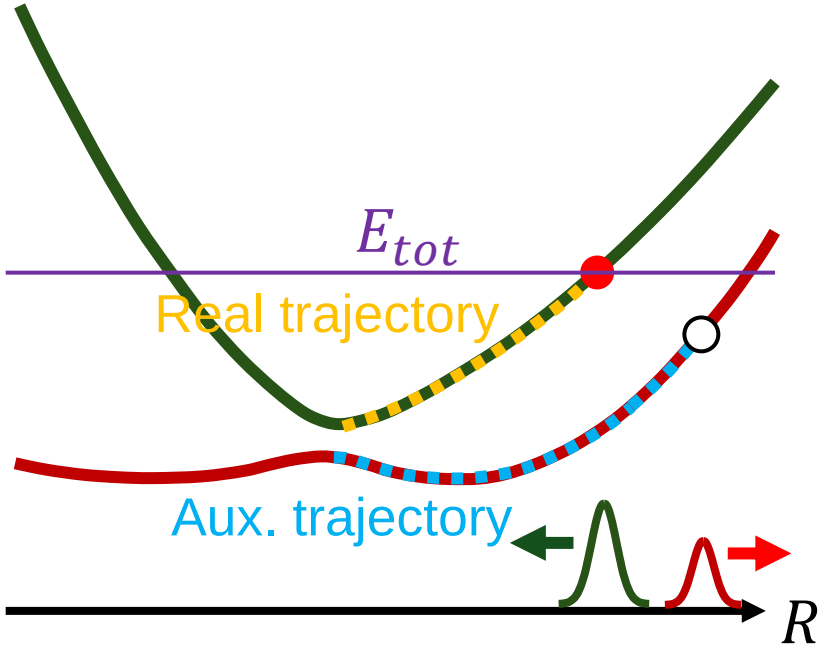

Case II. The real trajectory encounters the turning point.

Collapse the state to the active state.

These turning points could cause a jump in the total energy in mean-field based XF methods when processing the density matrix.

Ha, J.-K.; Min, S. K. JCP. ***2022***, 156 (17), 174109.

Arribas, E. V.; Vindel-Zandbergen, P.; Roy, S.; Maitra, N. T. PCCP. ***2023***, 25 (38), 26380–26395.

Independent-trajectory XF methods

- According to the approximation levels in the EOMs, the independent-trajectory XF methods are classified.
  - In SHXF (Surface Hopping based on XF), the electronic EOM is kept, while the nuclear evolution is simplified in the FSSH manner.
  - In MQCXF (Mixed Quantum-Classical based on XF), all XF terms are kept.
  - MFXF is the approximated version of MQCXF, neglecting the decoherence force.

Method	***Electronic EOM***	***Nuclear force***	***Velocity rescaling after a hop***	***Energy conservation***
SHXF	$H_{BO} + H_{XF}$	Active-state force	Yes	Yes
MQCXF		$F_{MF} + F_{XF}$	No	
MFXF		F_{MF}		No

Ha, J.-K.; Lee, I. S.; Min, S. K. JPCL. ***2018***, 9 (5), 1097–1104.

Ha, J.-K.; Min, S. K. JCP. ***2022***, 156 (17), 174109.

Arribas, E. V.; Vindel-Zandbergen, P.; Roy, S.; Maitra, N. T. PCCP. ***2023***, 25 (38), 26380–26395.

Calculation settings

- 5 model Hamiltonians are employed for assessing the XF methods.

- Conventional nonadiabatic dynamics methods such as Ehrenfest, FSSH, SDM and BCSH are employed as well for the comparative study.

- Exact discrete-variable representation (DVR) dynamics calculations are utilized as the reference.

Avg. position $\langle R(t)\rangle = \int dR\, R \sum_a |\chi_a(R,t)|^2 \approx \frac{1}{N_{tr}} \sum_k R^k(t)$

population $\langle \rho_i(t)\rangle = \int dR\ |\chi_i(R,t)|^2 \approx \frac{1}{N_{tr}} \sum_k \left|C_i^k(t)\right|^2$

coherence $\left\langle \left|\rho_{ij}\right|^2(t)\right\rangle = \int dR \frac{|\chi_i(R,t)|^2 \left|\chi_j(R,t)\right|^2}{\sum_a |\chi_a(R,t)|^2} \approx \frac{1}{N_{tr}} \sum_k \left|C_i^k(t)\right|^2 \left|C_j^k(t)\right|^2$

- All computations are conducted through the Libra package.

Calculation settings

- Model Hamiltonians

Extended Crossing with Reflection (ECWR) & Double Arch Geometry (DAG) → open

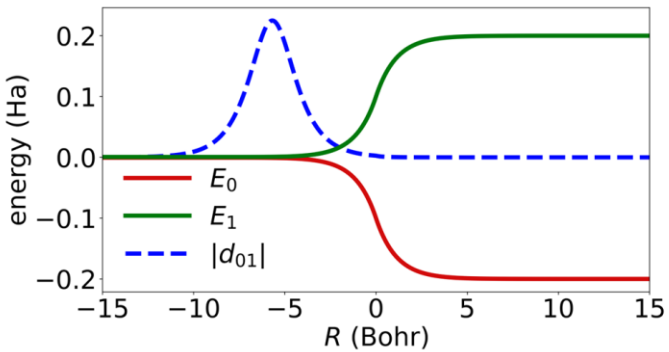

(a)

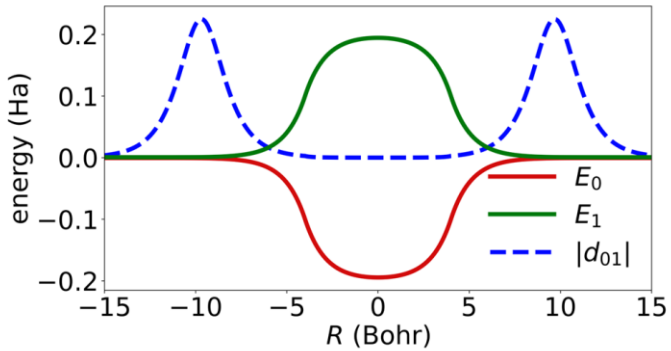

(b)

3-state Esch-Levine model → open & bound

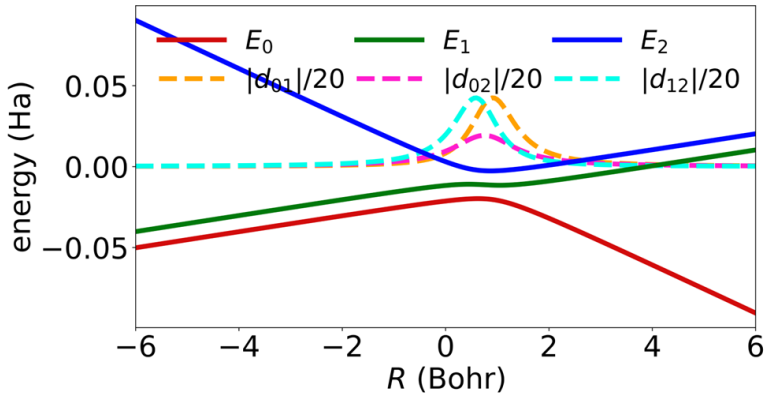

(e)

Single-Crossing (SC) and Double-Crossing (DC) Holstein → bound

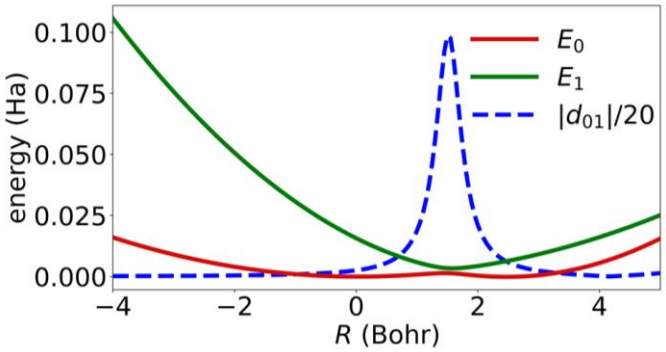

(c)

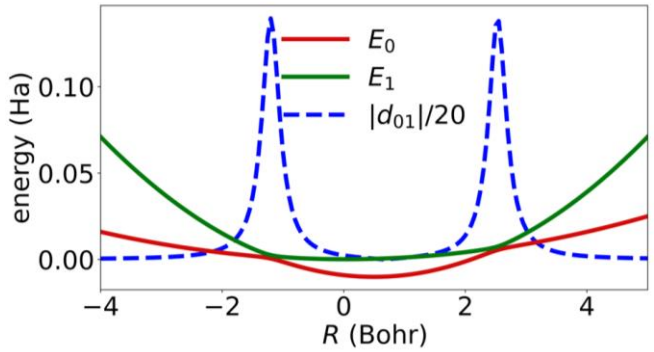

(d)

To consider a typical combination of nuclear motions and multiple crossings during the dynamics

ECWR and DAG

- Good testbeds for the implementation!

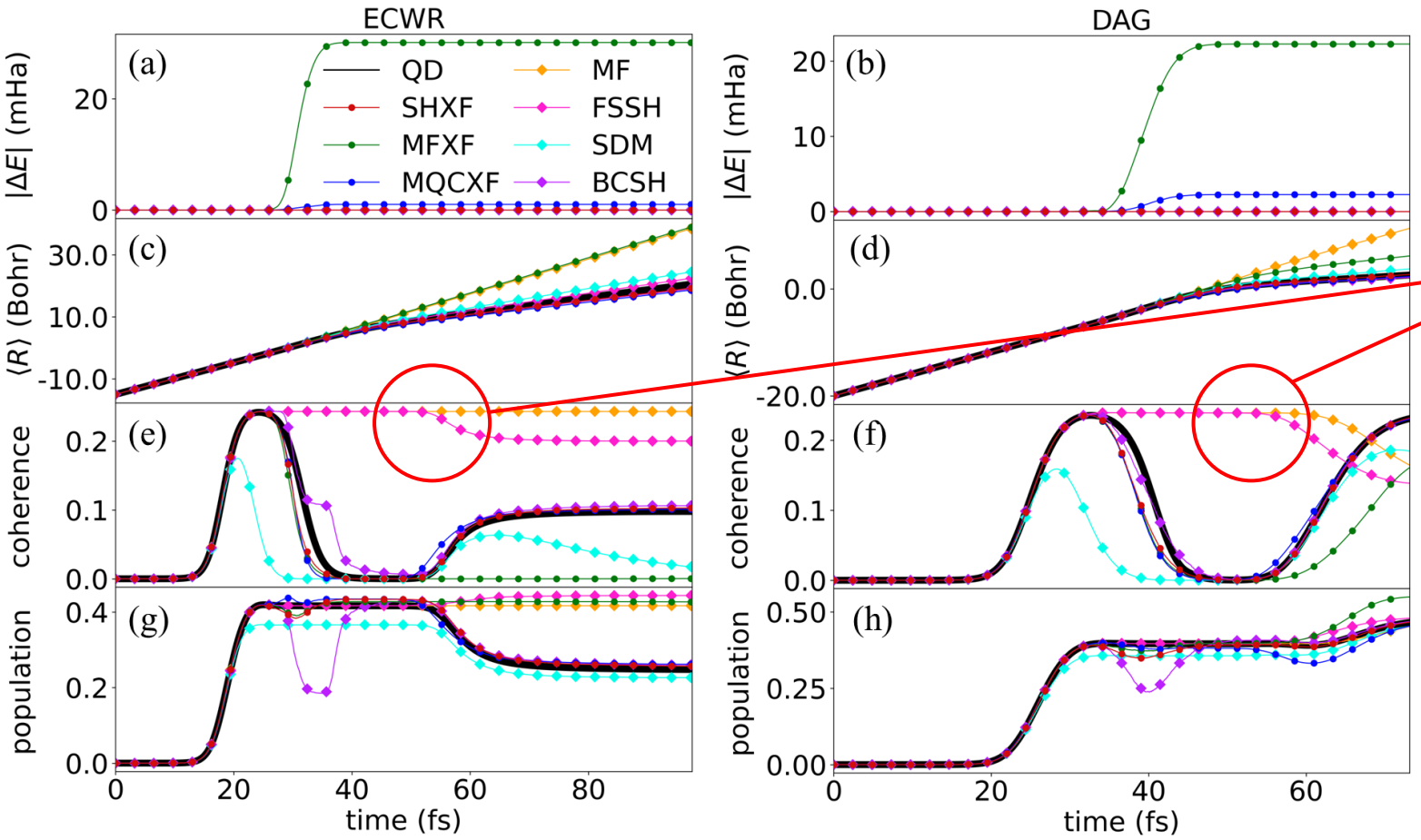

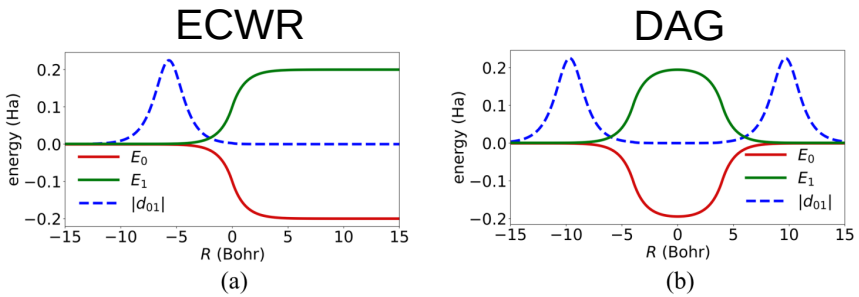

In the FSSH and Ehrenfest dynamics, overcoherence is shown after passing the NAC region

ECWR and DAG

- Good testbeds for the implementation!

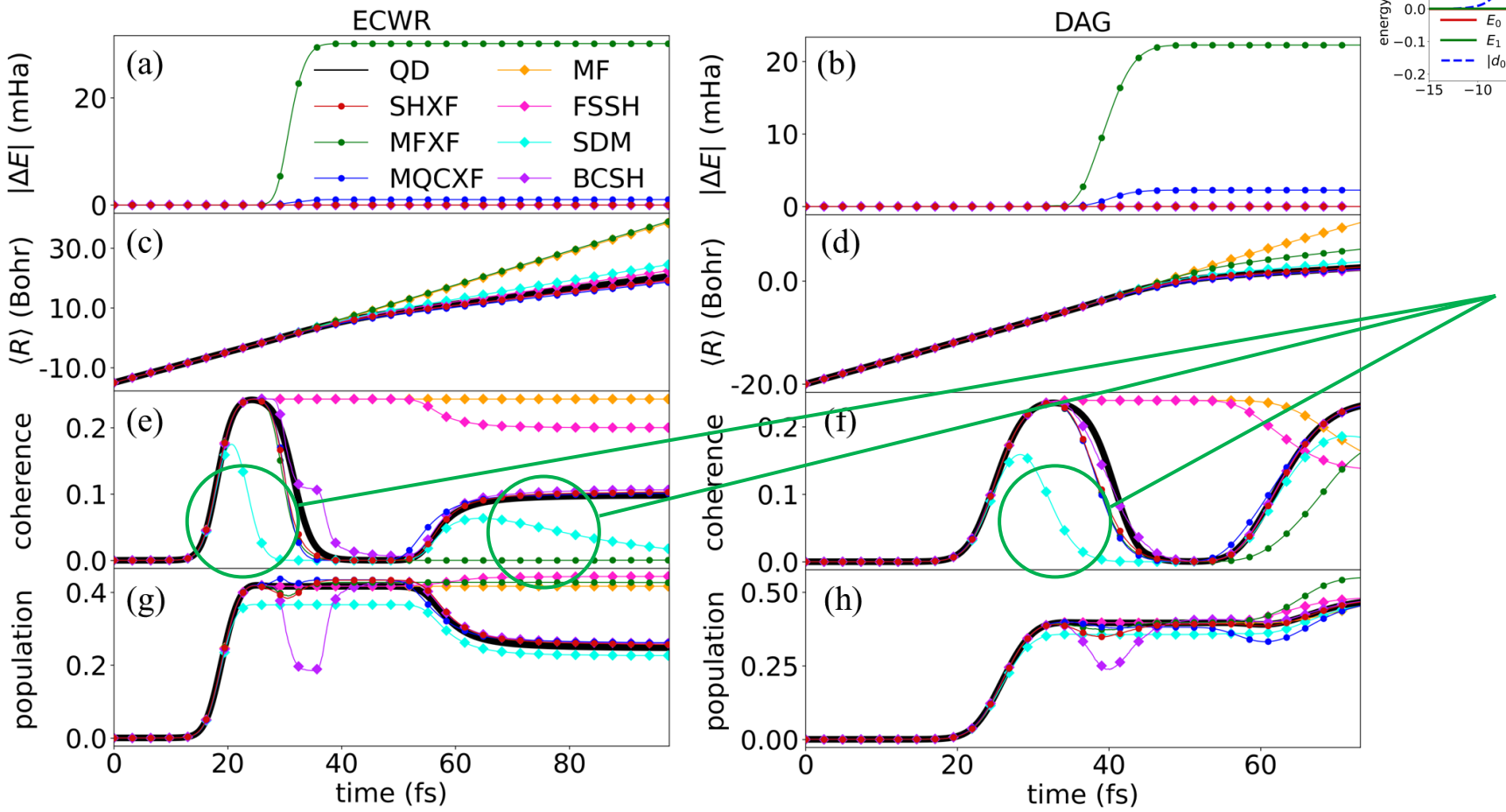

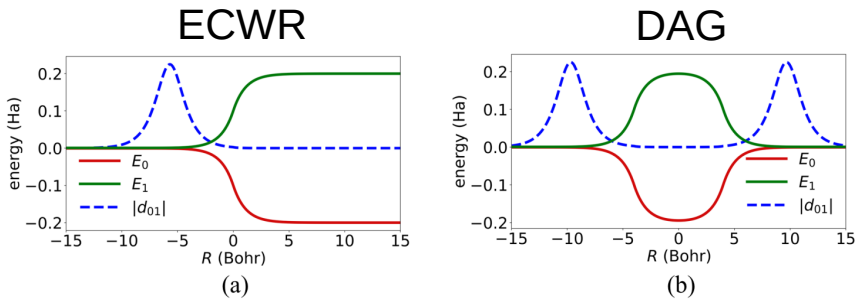

SDM shows the decoherence, whereas it shows the “undercoherence” and failed to describe the later coherence.

ECWR and DAG

- Good testbeds for the implementation!

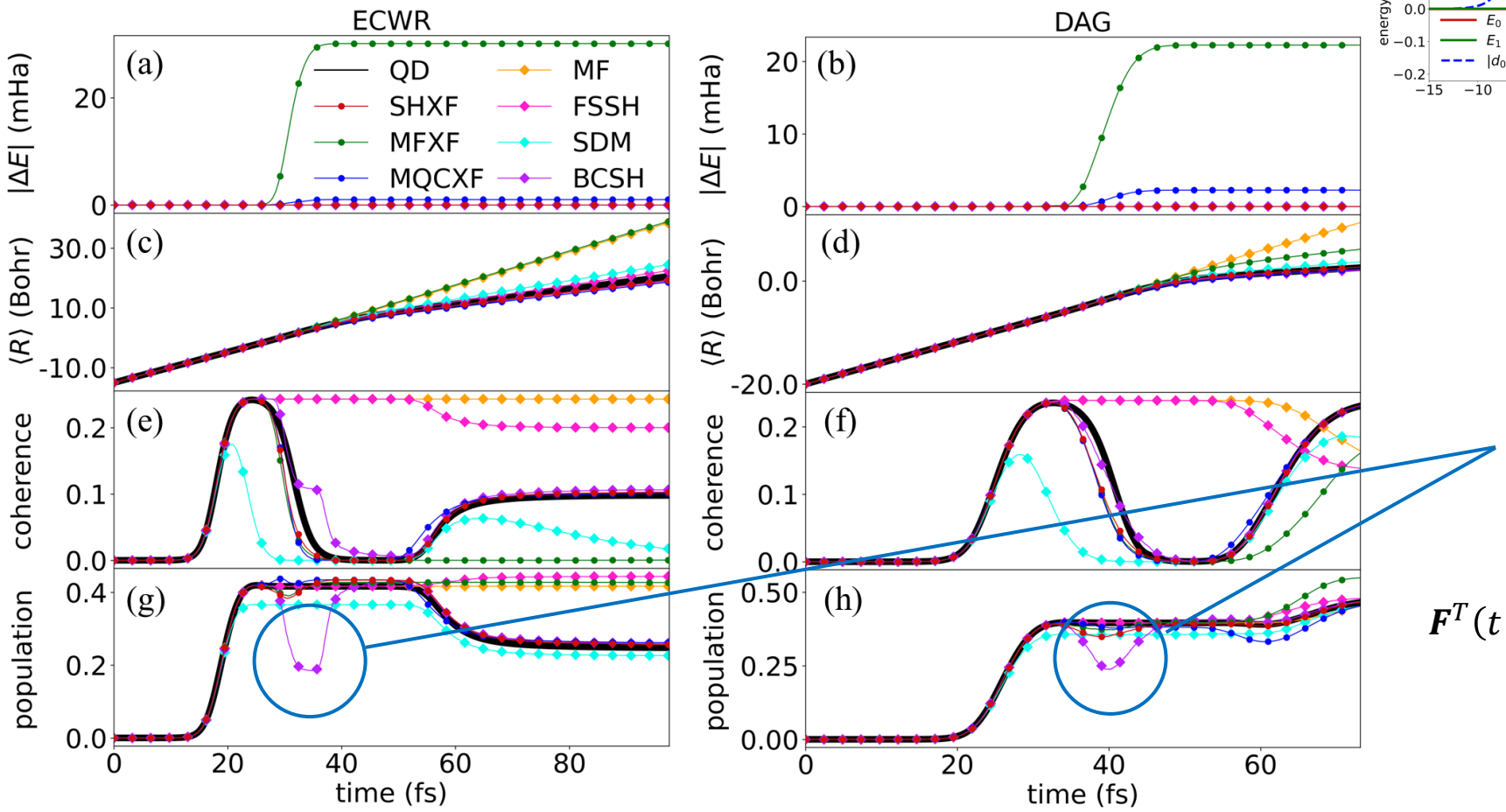

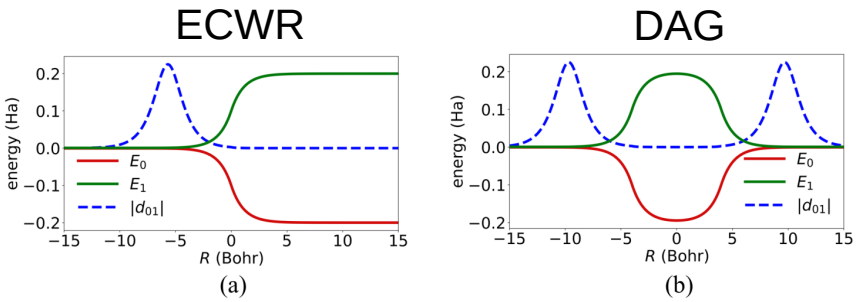

The population from BCSH shows bumps when the density collapse occurs at classical turning point.

$$\boldsymbol{F}^T(t+\Delta t)\boldsymbol{P}(t+\Delta t)\cdot\boldsymbol{F}^T(t+\Delta t)\boldsymbol{P}(t)<0$$

ECWR and DAG

- Good testbeds for the implementation!

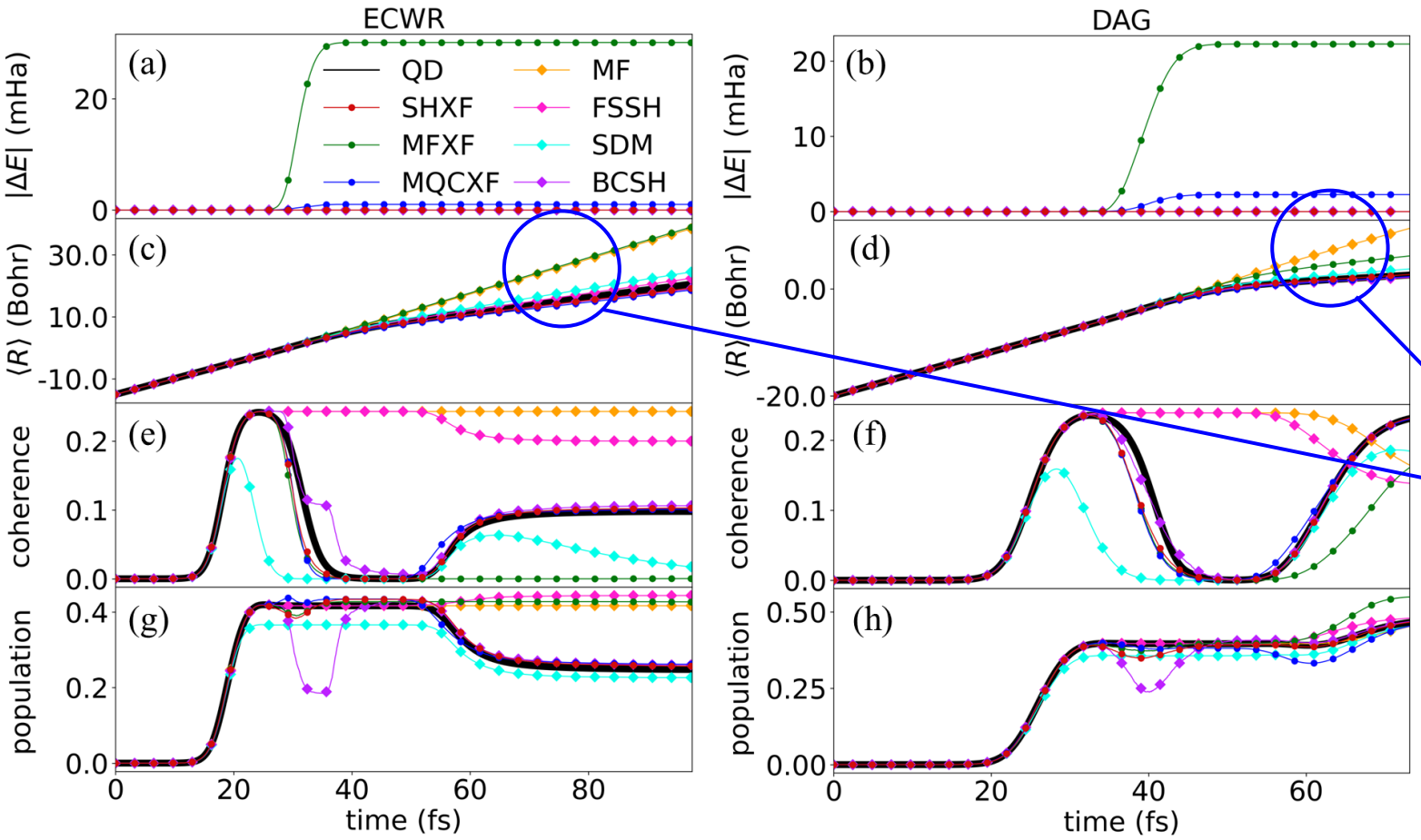

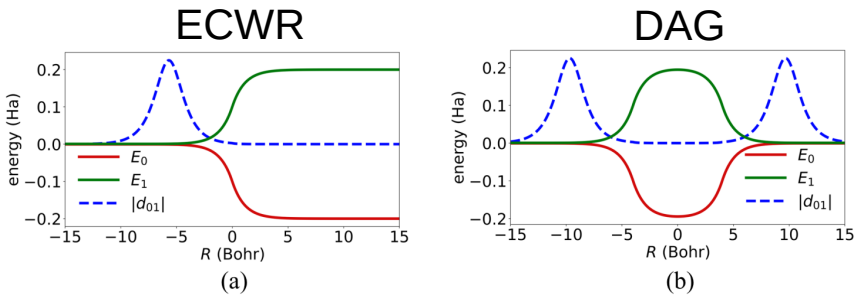

Ehrenfest and MFXF, in which the decoherence force is missing, show the deviation in describing the branching.

ECWR and DAG

- Good testbeds for the implementation!

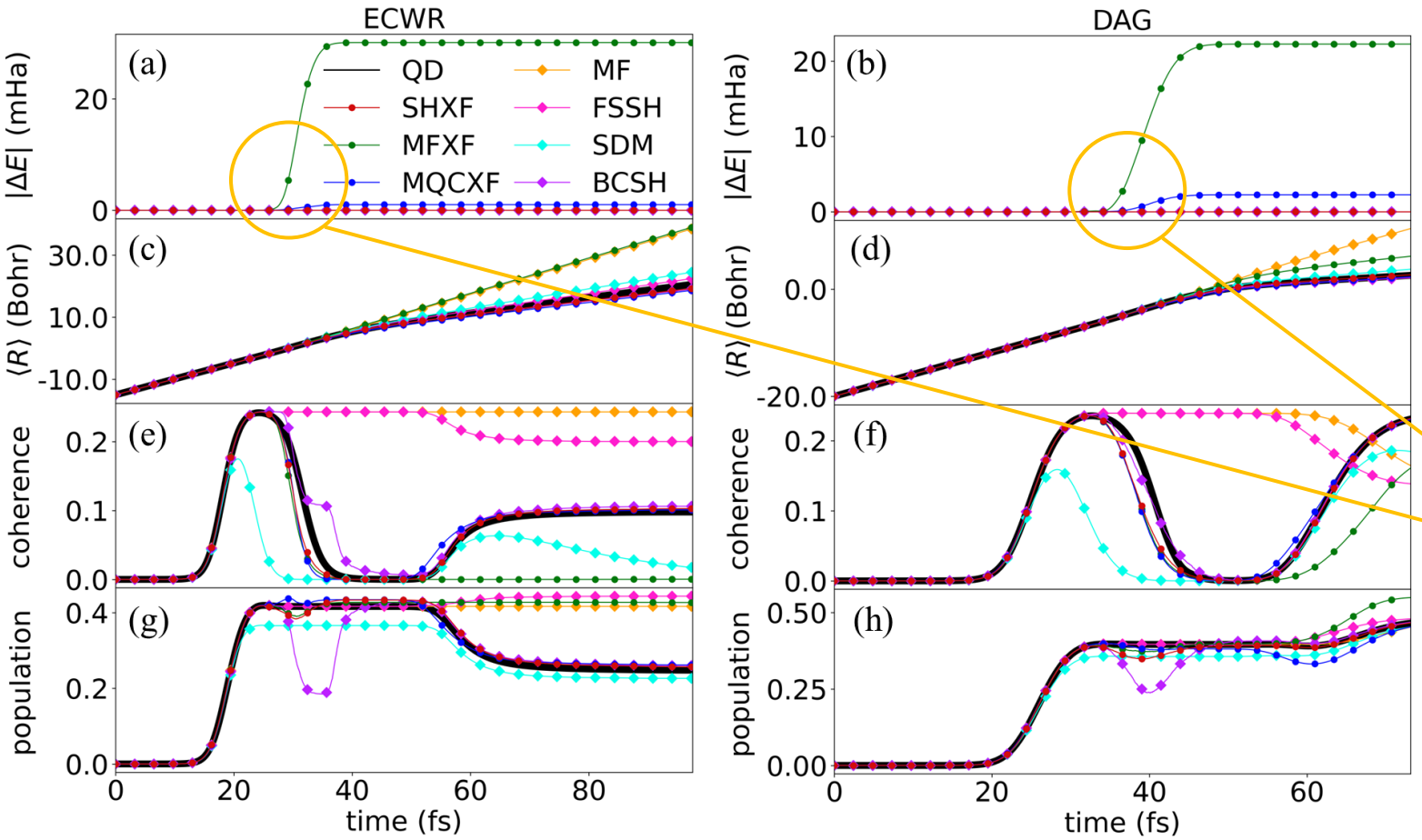

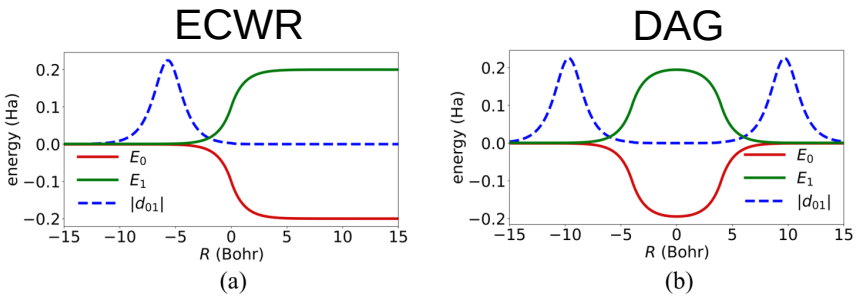

There are jumps of total energy in MQCXF. This extent is more severe in MFXF, since the energy conservation is not expected in the first place.

SC and DC Holstein model

- Multiple crossings in the bound systems

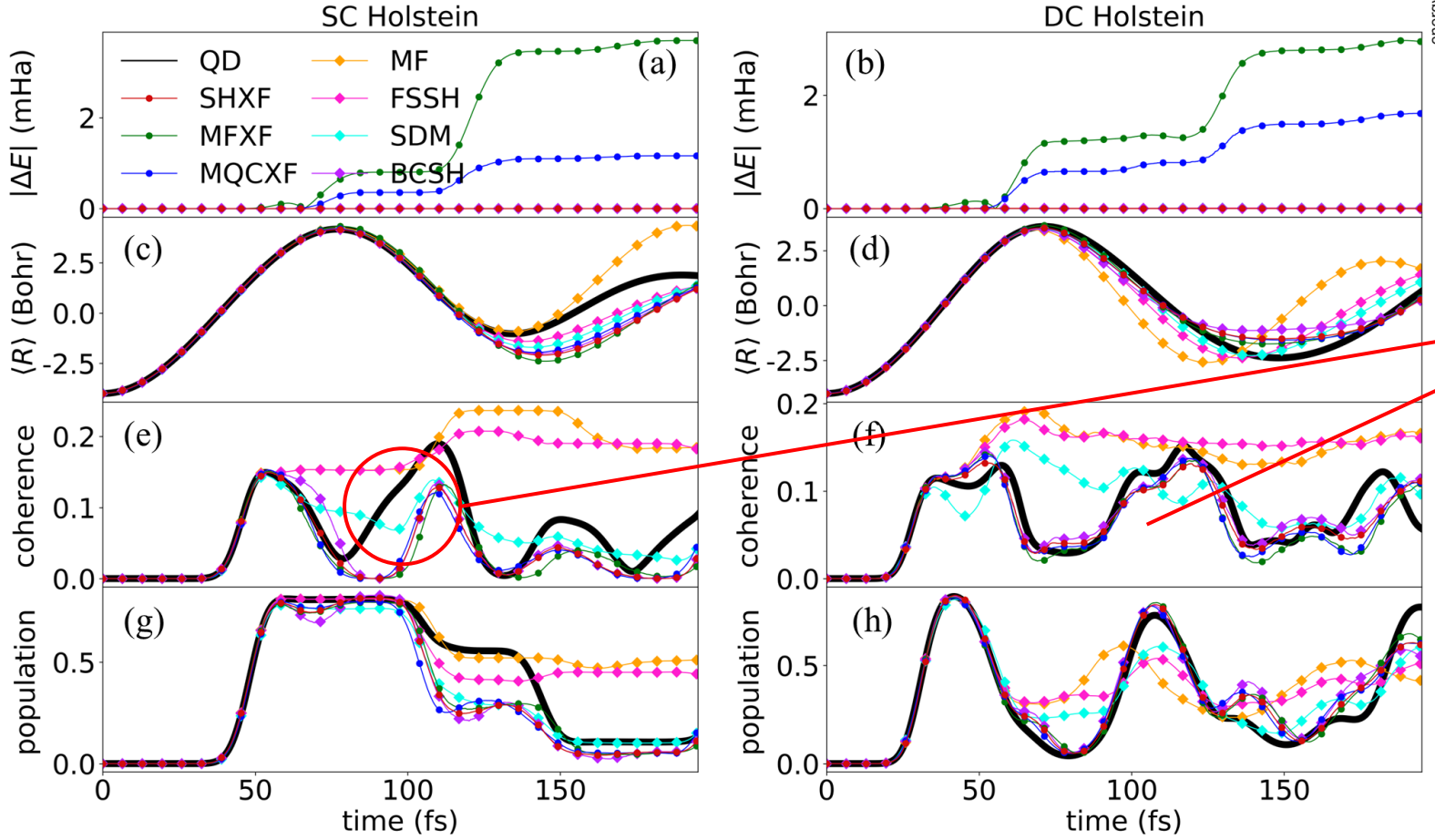

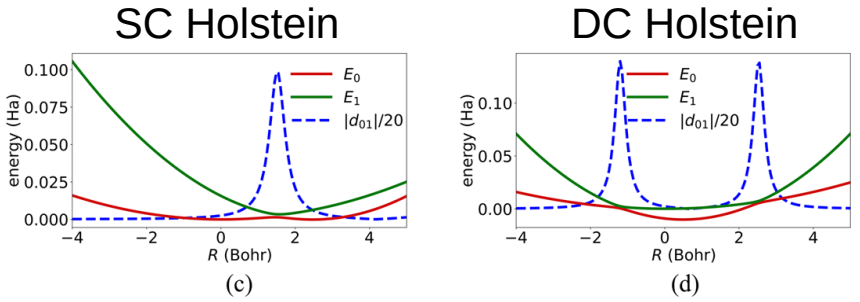

In the SC Holstein model, the deviation in coherence is more pronounced, since the effect of wavepacket overlap is more frequent.

SC and DC Holstein model

- The MQCXF snapshots of the SC Holstein model

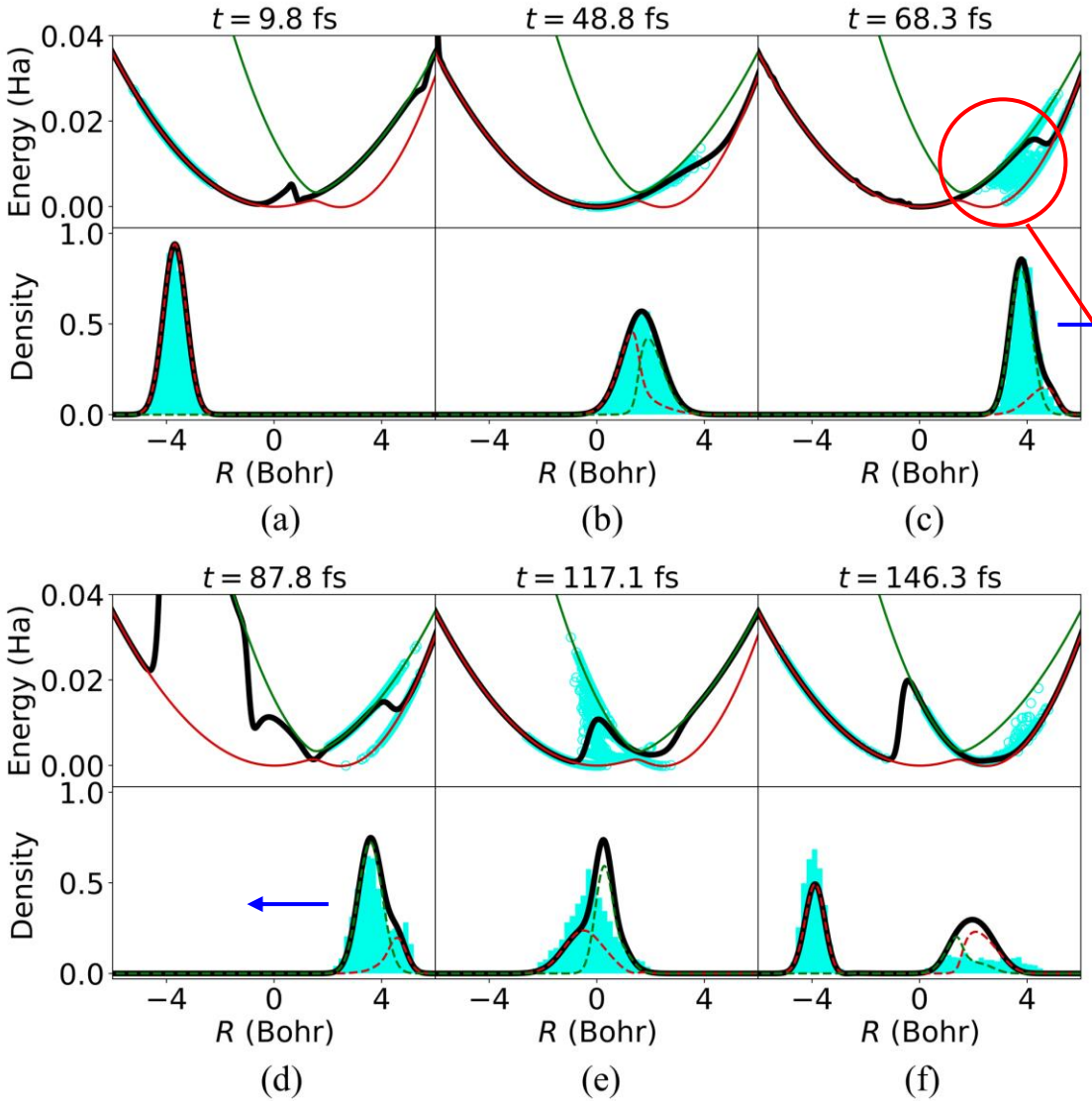

TDPES from the DVR dynamics

TDPES from the MQCXF method

$$\langle \Phi_R(t) | \hat{H}_{BO} | \Phi_R(t) \rangle = \frac{\sum_i |\chi_i(R,t)|^2 E_i(R)}{\sum_a |\chi_a(R,t)|^2} \approx \frac{1}{N_{tr}} \sum_i^{N_{tr}} |C_i^k(t)|^2 E_i^k$$

Cascading classical TDPES reflects on the step in the quantum TDPES.

SC and DC Holstein model

- The MQCXF snapshots of the SC Holstein model

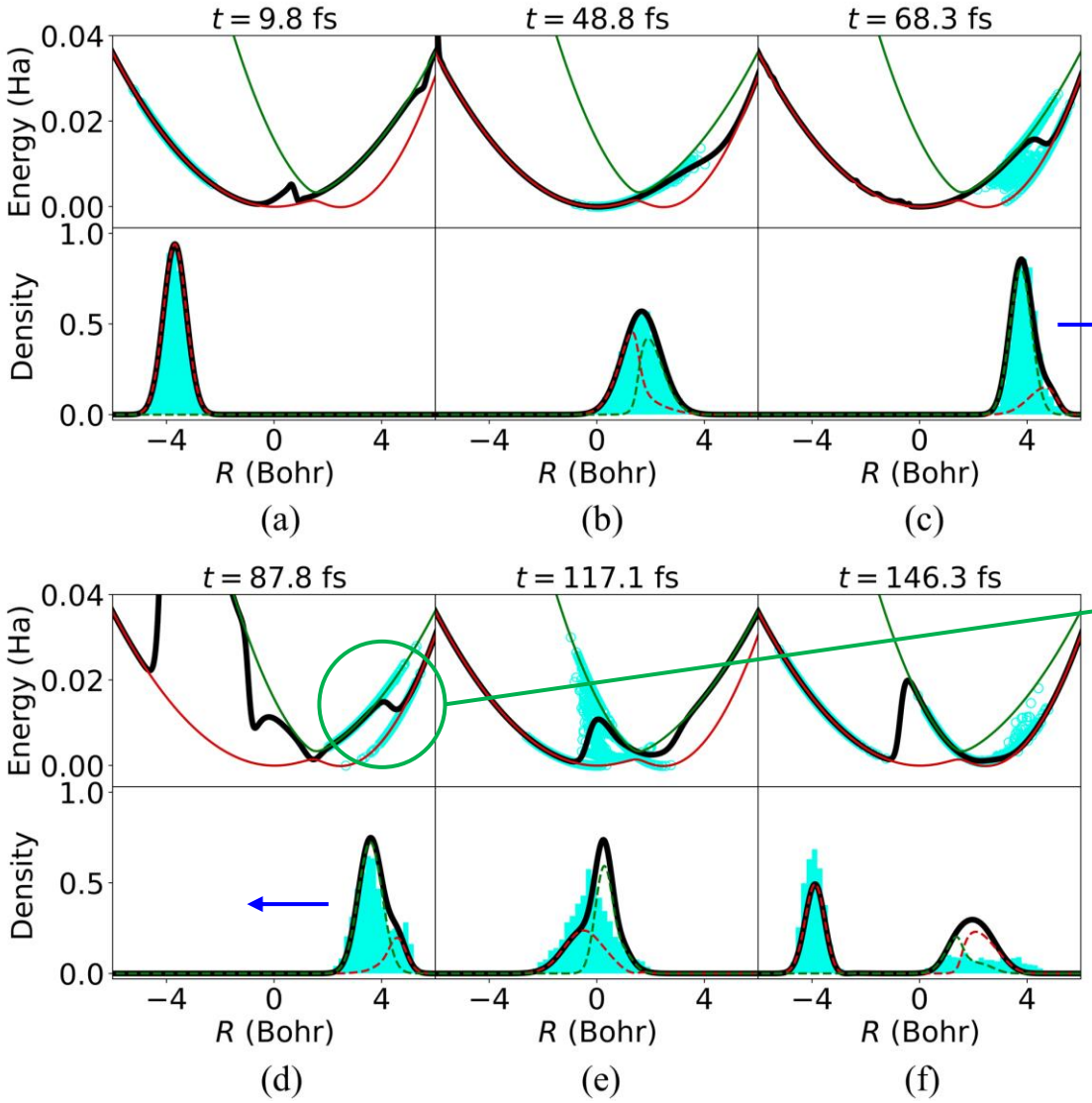

TDPES from the DVR dynamics

TDPES from the MQCXF method

$$\langle \Phi_R(t) | \hat{H}_{BO} | \Phi_R(t) \rangle = \frac{\sum_i |\chi_i(R,t)|^2 E_i(R)}{\sum_a |\chi_a(R,t)|^2} \approx \frac{1}{N_{tr}} \sum_i^{N_{tr}} |C_i^k(t)|^2 E_i^k$$

The MQC methods including MQCXF cannot describe the coherence from a pure overlap.
→ missing coherence pattern in the descriptor.

Classical positions on each adiabatic state behave independent branches.

SC and DC Holstein model

- The MQCXF snapshots of the SC Holstein model

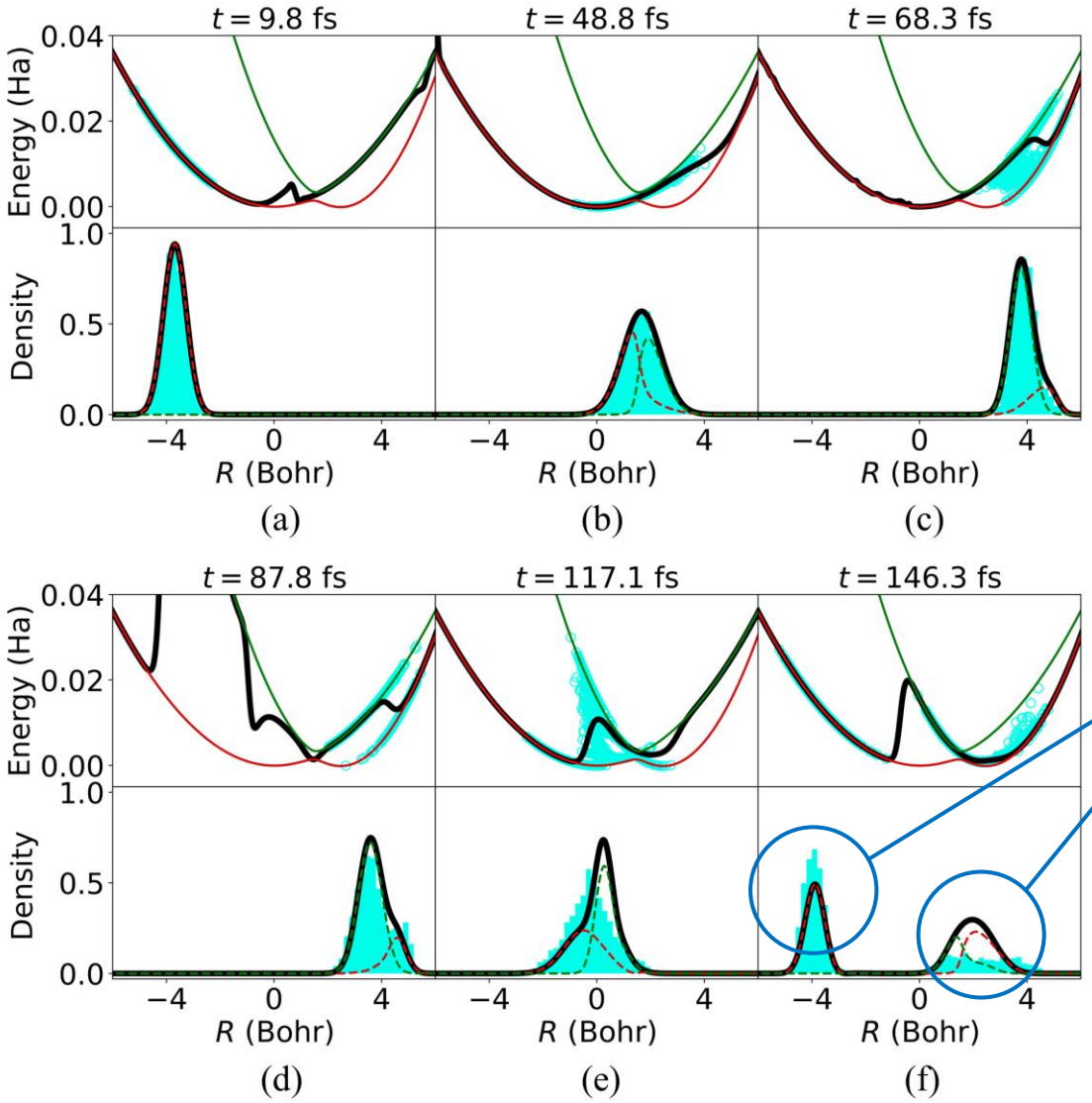

TDPES from the DVR dynamics

TDPES from the MQCXF method

$$\langle \Phi_R(t) | \hat{H}_{BO} | \Phi_R(t) \rangle = \frac{\sum_i |\chi_i(R,t)|^2 E_i(R)}{\sum_a |\chi_a(R,t)|^2} \approx \frac{1}{N_{tr}} \sum_i^{N_{tr}} |C_i^k(t)|^2 E_i^k$$

Missing coherence in the middle of the dynamics eventually leads to the wrong branching ratio.

Esch-Levine model

- Open + bound: A multistate example of (de)coherence

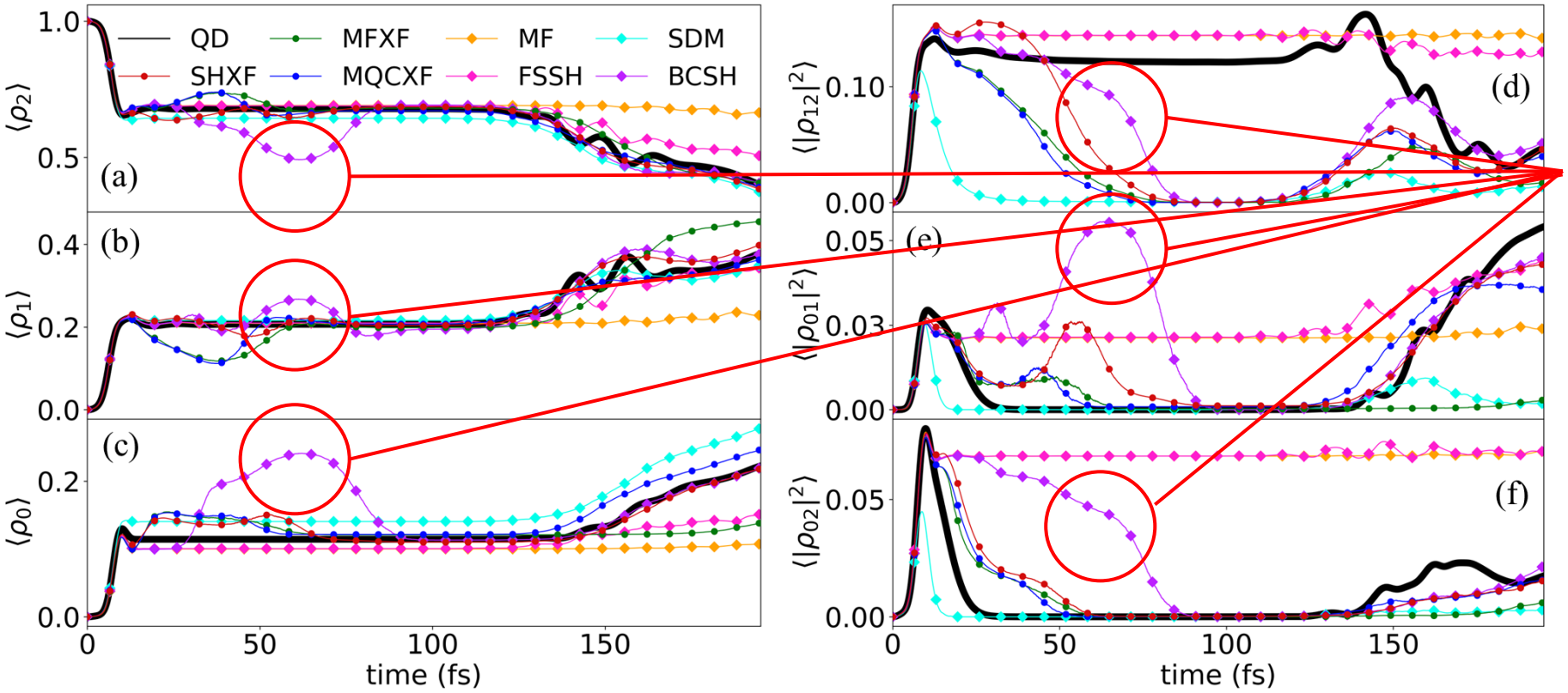

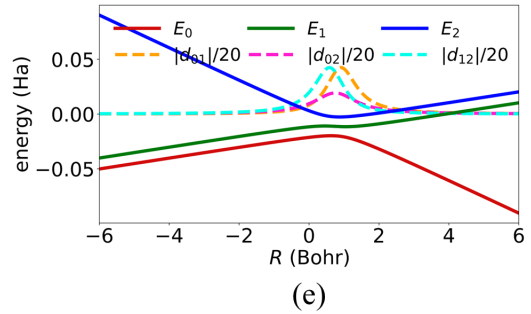

(e)

BCSH shows the bumps as in the ECWR and DAG models due to the abrupt collapse of density in the turning point.

Esch-Levine model

- Open + bound: A multistate example of (de)coherence

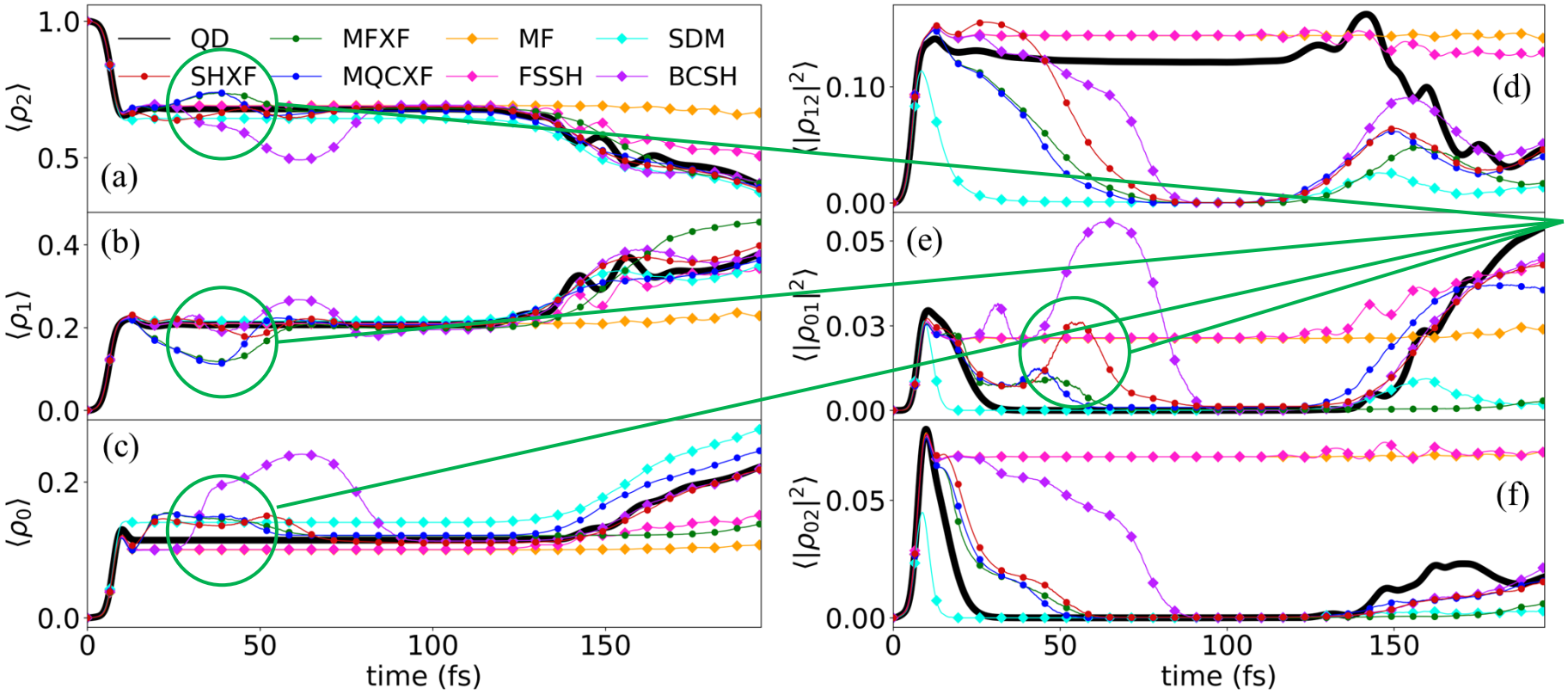

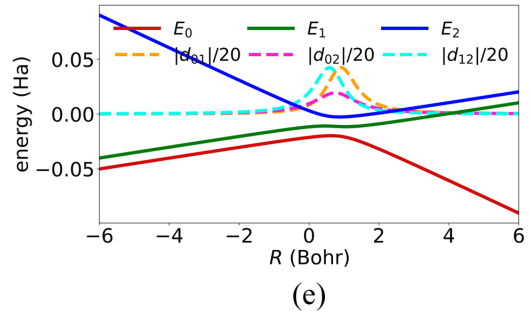

Due to the BC feature, a similar pattern is found as well, while the drift is less pronounced, since the electronic EOM contains the decoherence directly.

Esch-Levine model

- Open + bound: A multistate example of (de)coherence

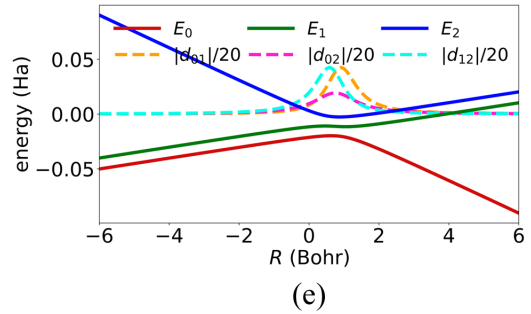

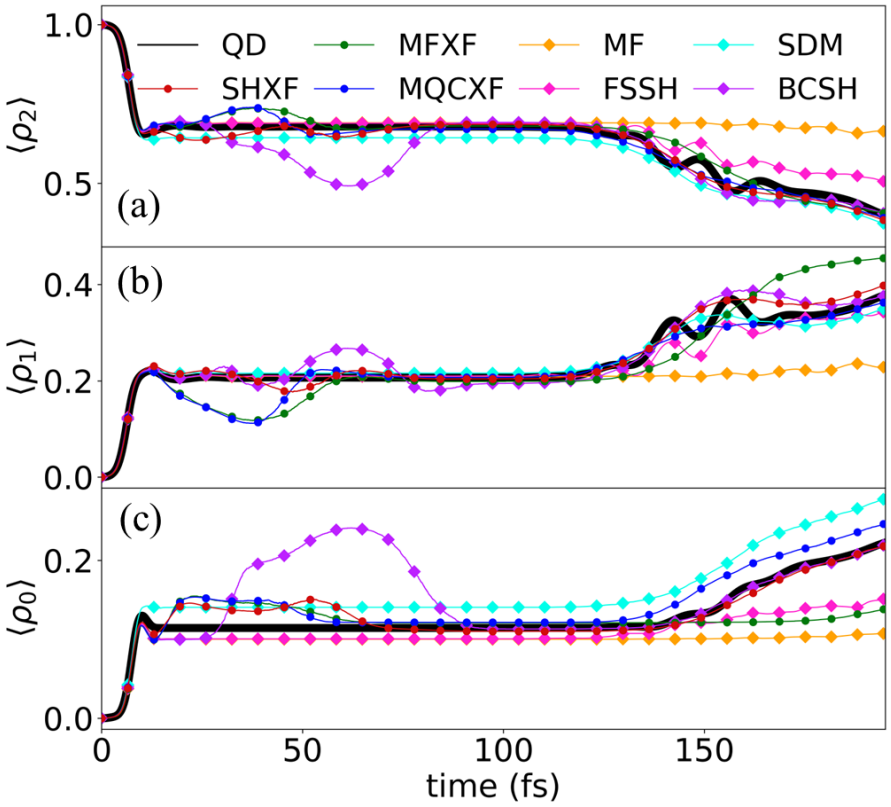

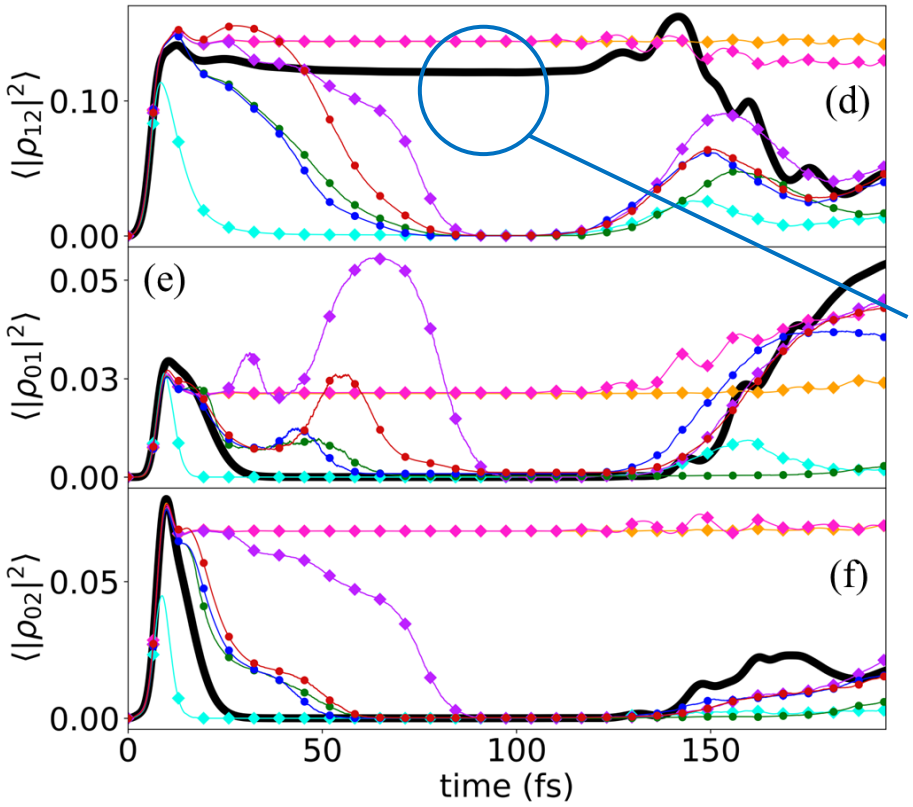

The coherence due to the wavepacket overlap cannot be fully described.

Esch-Levine model

- The MQCXF snapshots

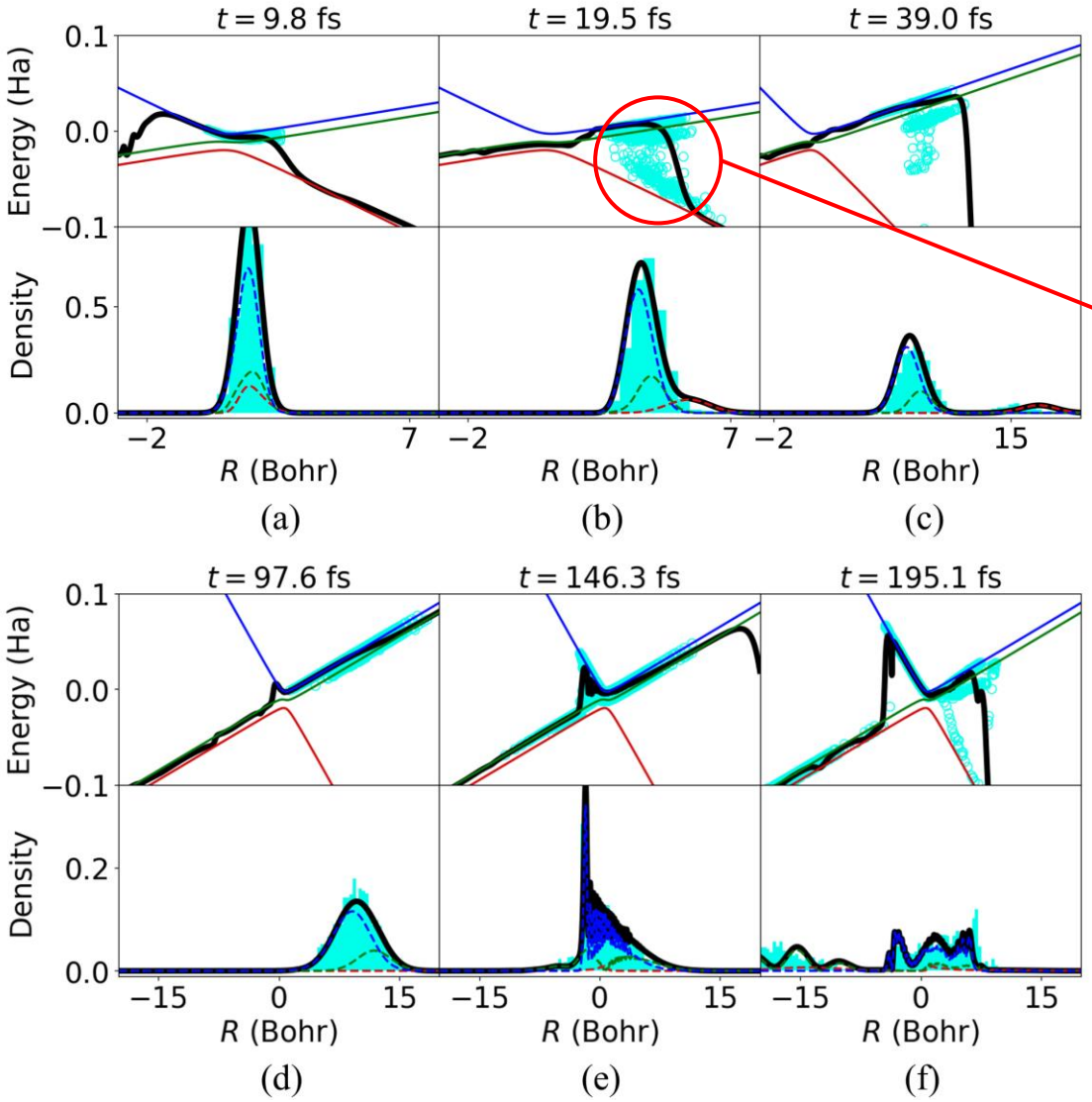

Cascading classical TDPES reflects on the step in the quantum TDPES.

Esch-Levine model

- The MQCXF snapshots

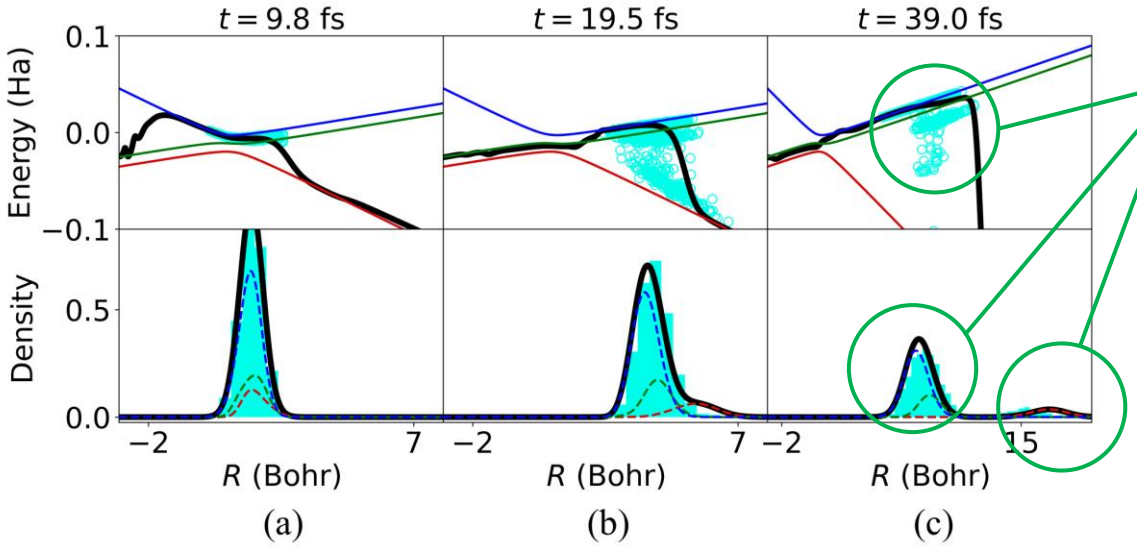

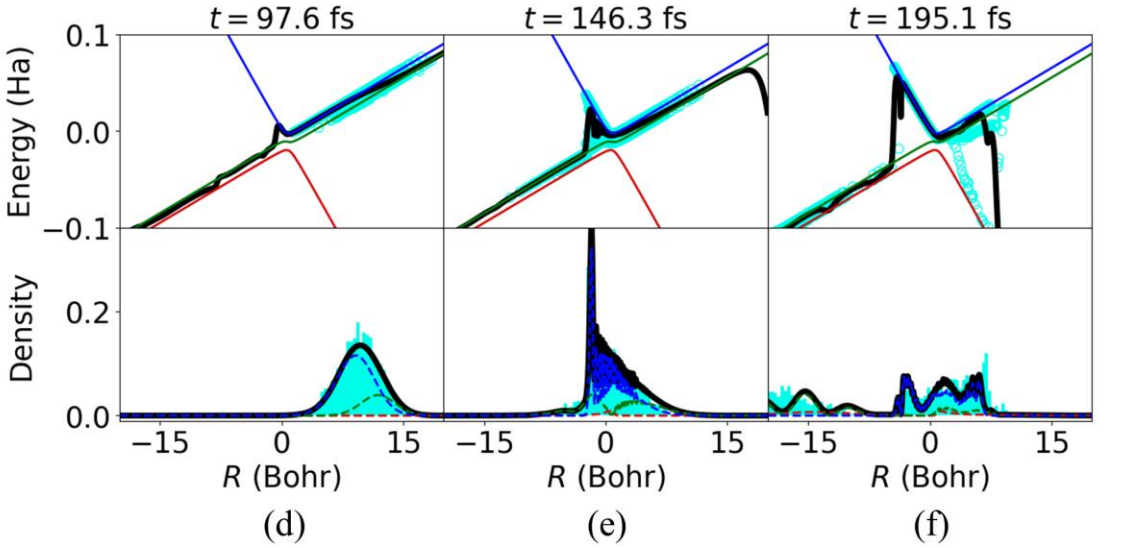

Decoherence in wavepacket and branching

Esch-Levine model

- The MQCXF snapshots

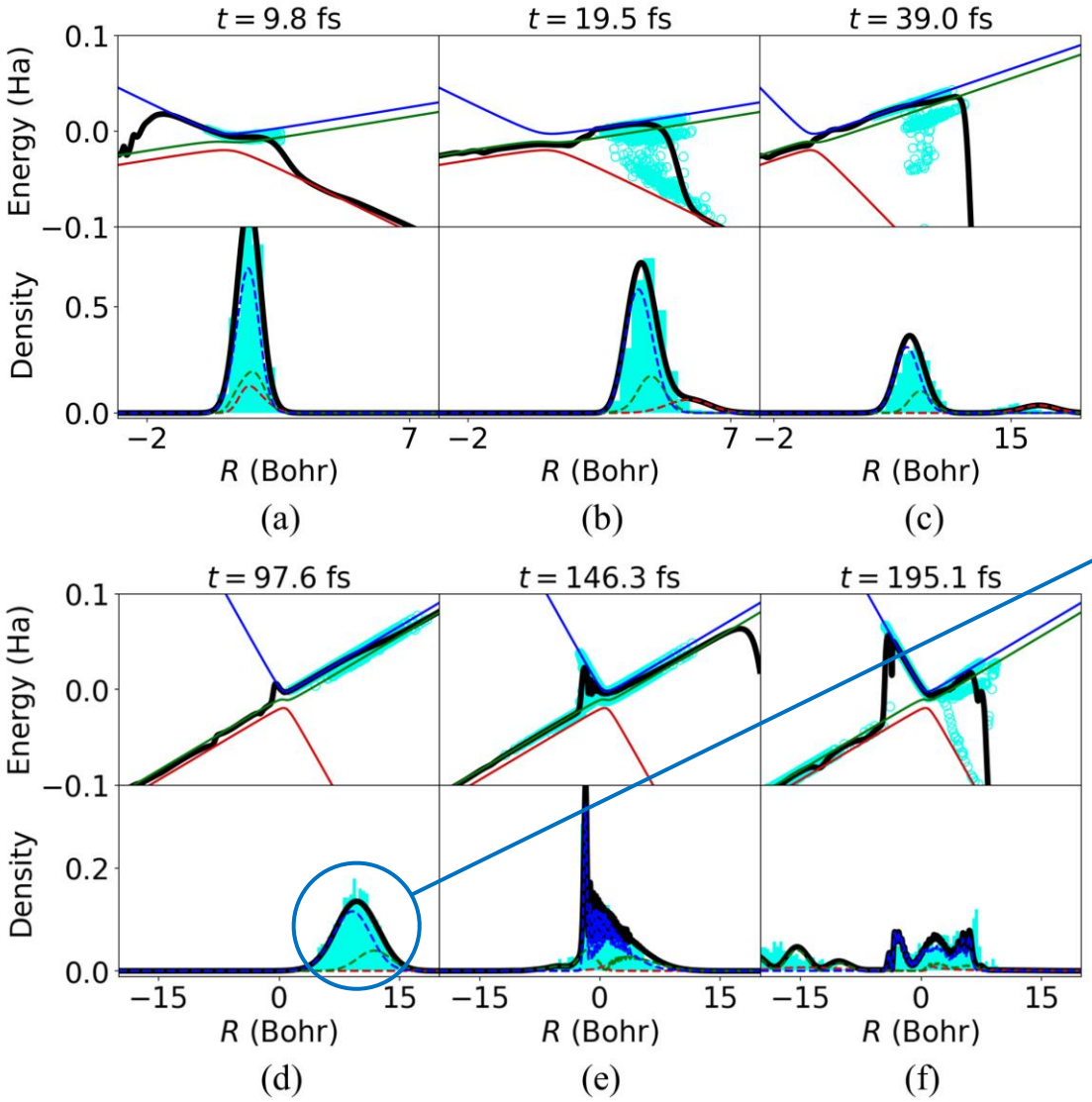

This wavepacket overlap is missing in the MQC dynamics.

Esch-Levine model

- The MQCXF snapshots

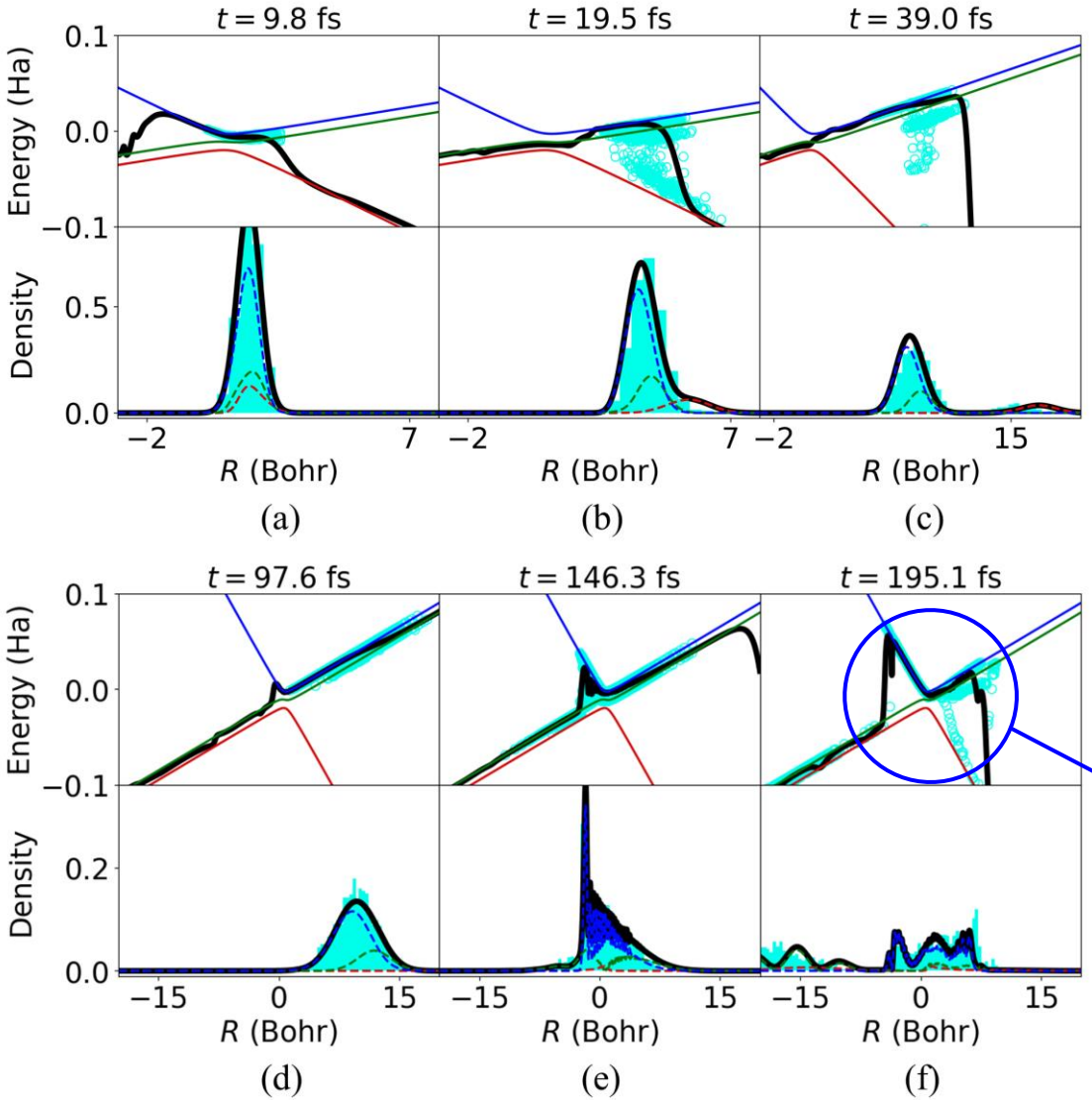

Classical positions on each branch lose its coherence, and behave individually.

Method assessment

- The accuracy metrics from the mean square error

$$\epsilon_{\mathrm{SH/SE,pop}} = \frac{1}{N_{steps} \times N} \sum_{a=0}^{N_{steps}-1} \sum_{i=0}^{N-1} \left[\langle \rho_i(t_a) \rangle_Q - \langle \rho_i(t_a) \rangle_{MQC}^{SH/SE} \right]^2 \qquad \epsilon_{coh} = \frac{2}{N_{steps} \times N(N-1)} \sum_{a=0}^{N_{steps}-1} \sum_{\substack{i,j=0 \\ i<j}}^{N-1} \left[\left\langle |\rho_{ij}|^2(t_a) \right\rangle_Q - \left\langle |\rho_{ij}|^2(t_a) \right\rangle_{MQC} \right]^2$$

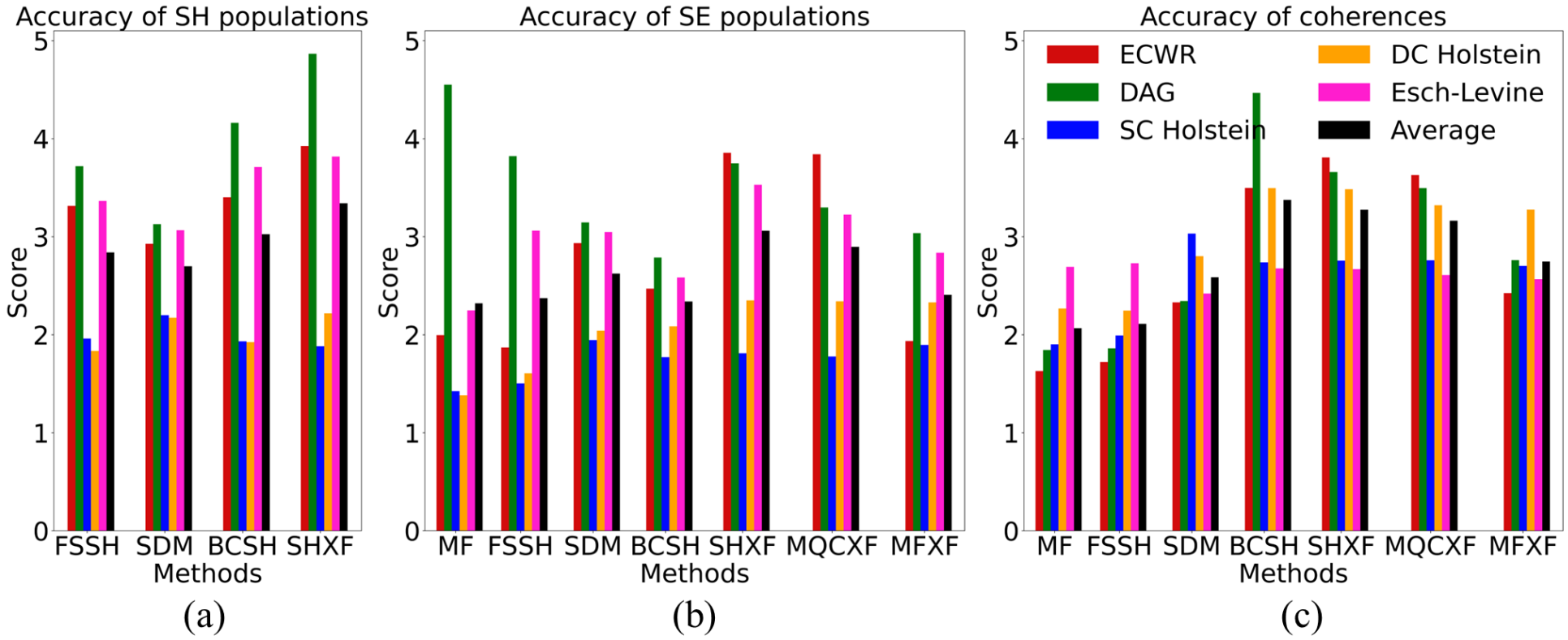

Population scores: SHXF > MQCXF > BCSH > SDM ≈ MFXF > FSSH ≈ MF

Coherence scores: BCSH > SHXF > MQCXF > MFXF > SDM > FSSH ≈ MF

Summary

- The traditional methods without the decoherence correction, FSSH and MF, causes the overcoherence.
- While the SDM method shows the decoherence, it yields undercoherence and has difficulty in describing the later coherence.
- There are spurious bumps in population and coherence within the branching correction, this effect can be diminished by applying the XF-based decoherence correction.
- The SHXF, MQCXF and BCSH methods show the most consistent and reliable results among the current set of model Hamiltonians.

Decoherence correction in the nonadiabatic dynamics

- "Overcoherence" problem: the decoherence is missing in the original electronic TDSE.

$$\dot{C}_i = -\frac{i}{\hbar} E_i C_i - \sum_j C_j \sum_\nu \dot{R}_\nu \cdot d_{ij,\nu}$$

0

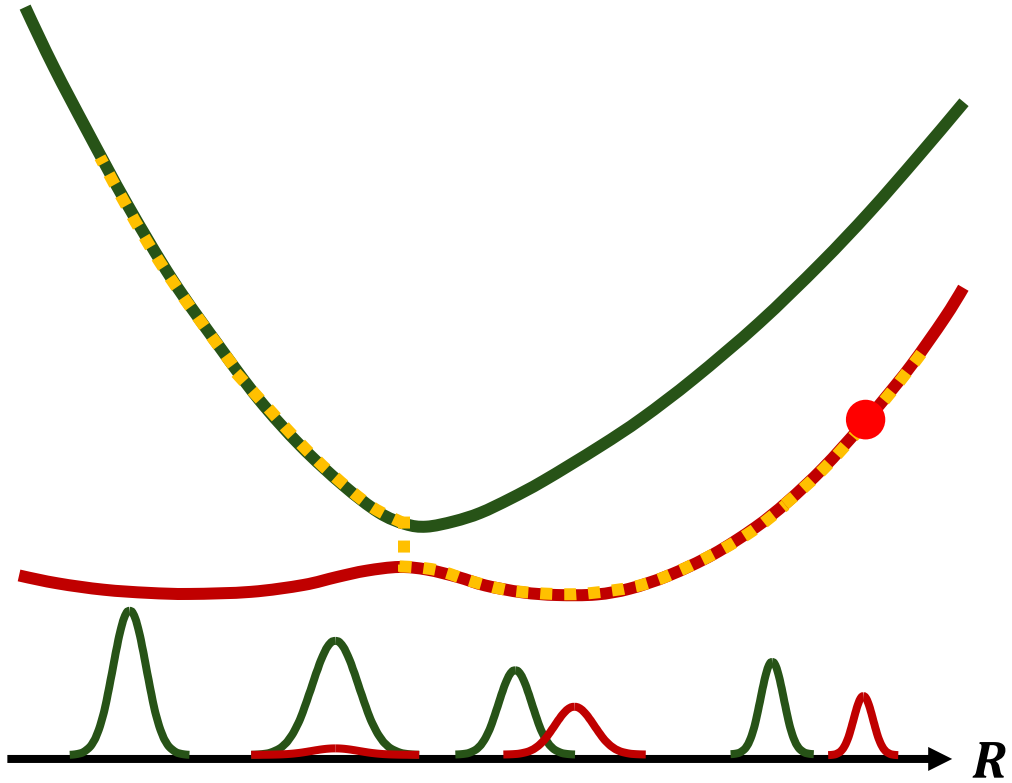

$$P_i = |C_i|^2$$